
Hidden Markov models are recurrent neural networks: A disease progression modeling application

Matt Baucum

Industrial & Systems Engineering
University of Tennessee Knoxville
Knoxville, TN 37996
mbaucum1@vols.utk.edu

Anahita Khojandi

Industrial & Systems Engineering
University of Tennessee Knoxville
Knoxville, TN 37996
khojandi@utk.edu

Theodore Papamarkou

Computational Sciences and Engineering Division
Oak Ridge National Laboratory
Oak Ridge, TN 37831
papamarkout@ornl.gov

Abstract

Hidden Markov models (HMMs) are commonly used for sequential data modeling when the true state of the system is not fully known. We formulate a special case of recurrent neural networks (RNNs), which we name hidden Markov recurrent neural networks (HMRNNs), and prove that each HMRNN has the same likelihood function as a corresponding discrete-observation HMM. We experimentally validate this theoretical result on synthetic datasets by showing that parameter estimates from HMRNNs are numerically close to those obtained from HMMs via the Baum-Welch algorithm. We demonstrate our method's utility in a case study on Alzheimer's disease progression, in which we augment HMRNNs with other predictive neural networks. The augmented HMRNN yields parameter estimates that offer a novel clinical interpretation and fit the patient data better than HMM parameter estimates from the Baum-Welch algorithm.

1 Introduction

Hidden Markov models (HMMs; [1]) are commonly used for modeling disease progression, because they allow researchers to conceptualize complex (and noisy) clinical measurements as originating from a smaller set of latent health states (typically discrete). Each latent health state is characterized by an emission distribution that specifies the probabilities of each measurement/observation given that state. This allows HMMs to explicitly account for uncertainty or measurement error, since the system's true state is not fully observable. Because of their intuitive parameter interpretations and flexibility, HMMs have been used to model biomarker changes in HIV patients [2], Alzheimer's disease progression [3], breast cancer screening decisions [4], and patient response to blood anticoagulants [5].

For certain health applications, researchers may wish to integrate HMMs with other disease progression models and/or data sources. For instance, researchers in [6] jointly trained parameters for a partially-observable Markov decision process and a reinforcement learning policy to maximize patient returns. Other researchers have attempted to learn or initialize HMM parameters based on additional sources of patient data; [7] presents a procedure for initializing HMM parameters from limited information about patient health states, while [8] learned a cancer progression HMM where the transition probabilities depend on patient-level covariates. Such HMM modifications typically require multiple estimation steps (e.g., [8]) or changes to parameter interpretation (e.g., [6]). This

is because the algorithm for fitting HMMs, the Baum-Welch algorithm [1], is strictly designed to maximize the likelihood of a data sequence without consideration of additional covariates.

In this work, we introduce Hidden Markov Recurrent Neural Networks (HMRNNs) - neural networks that mimic the computation of hidden Markov models while allowing for substantial modularity with other predictive networks. Unlike past work combining neural networks and HMMs (e.g., [9]), HMRNNs are not domain-specific, and are designed to maximize the most commonly-used HMM fit criterion - the likelihood of the data given the parameters. In doing so, our primary contributions are as follows: (1) We prove how recurrent neural networks (RNNs) can be formulated to optimize the same likelihood function as HMMs, with parameters that can be interpreted as HMM parameters; (2) We show how HMMs formulated as neural networks can easily ‘plug in’ to other neural networks, allowing for one-step estimation of robust predictive models; (3) We demonstrate our model’s utility in a disease progression application, in which it improves predictive accuracy and offers unique parameter interpretations not afforded by simple HMMs.

2 Related work

There exists a limited but growing literature that explores the integration of HMMs and neural networks, mostly with applications in speech analysis and handwriting recognition. [10], [11], and [12] combined HMMs and neural networks for handwriting recognition. [10] used HMM outputs as the inputs for a neural network to identify fraudulent signatures, while [12] used HMM outputs as the targets for training a neural network to recognize cursive handwriting. In [11], researchers combined HMM and RNN outputs to learn complementary text features. [13] jointly optimized an HMM/neural network hybrid for speech recognition, with the neural network supplying the HMM input sequences. [14] uses HMMs to interpret the hidden state representations from RNNs trained on language data. Although this literature is somewhat related to our work, it does not focus on casting HMMs as neural networks, the subject of our study.

A smaller number of studies have attempted to formally model HMMs in a neural network context. Researchers in [15] proposed using neural networks to approximate Gaussian emission distributions in HMMs; however, their method requires pre-training of the HMM and merely uses the neural network to ‘refine’ the emission parameters. Similar to our work, [9] demonstrated how HMMs can be reduced to recurrent neural networks for speech recognition, though it requires that neurons be computed via products (rather than sums), which are not commonly used in modern neural networks. Furthermore, the model in [9] maximizes the mutual information between observations and hidden states; this is a commonly used criterion in speech recognition, but less common than likelihood maximization in other domains (e.g., disease progression modeling). Lastly, [9] and [15] presented only theoretical justification, with no empirical comparisons with the Baum-Welch algorithm. In contrast with past work, we formulate an HMM that can be fully trained as a neural network, employs widely-used neural network operations, maximizes the observed data’s likelihood, and compares favorably to the Baum-Welch algorithm when tested on real-world datasets.

A limited number of studies have also explored connections between neural networks and Markov models in the healthcare domain. For instance, [5] employed a discriminative hidden Markov model to estimate ‘hidden states’ underlying patients’ ICU measurements, though these hidden states were not mathematically equivalent to HMM latent states. In another study, [16] compared HMM and neural network effectiveness in training a robotic surgery assistant. Both models were used to recognize and predict surgeons’ movements, with the neural network offering increased accuracy and the HMM offering reduced computational complexity. [17] proposed a generative neural network for modeling ICU patient health. The model was used for training reinforcement learning treatment policies, and was based on the core principles of HMMs. Although these studies showcase the value of pairing neural networks and Markov models in the healthcare domain, they differ from our approach of directly formulating HMMs as neural networks, which maintains the interpretability of HMMs while allowing for joint estimation of the HMM with other predictive models.

In summary, while these studies have shown the promise of incorporating elements of HMMs into deep learning tasks, there are no existing methods for optimizing HMM log-likelihood in a neural network context. Implementing HMMs as neural networks maintains their interpretability, while allowing additional data sources (e.g., patient covariates) to steer model estimation to better-fitting solutions.

and an Alzheimer’s disease progression case study of public clinical data. Finally, in Section 5 we discuss the findings and future work.

3 Methods

In this section, we briefly review HMM preliminaries, formally define the HMRNN, and prove that it optimizes the same likelihood function as a corresponding HMM.

3.1 HMM preliminaries

Formally, an HMM models a system over a given time horizon T , where the system occupies a hidden state $x_t \in S = \{1, 2, \dots, k\}$ at any given time point $t \in \{0, 1, \dots, T\}$; that is, $x_t = i$ indicates that the system is in the i th state at time t . For any state $x_t \in S$ and any time point $t \in \{0, 1, \dots, T\}$, the system emits an observation according to an emission distribution that is uniquely defined for each state. We consider the case of categorical emission distributions, which are commonly used in healthcare (e.g., [3, 18, 4, 19]). These systems emit one of c distinct observations at each time point; that is, for any time t , we observe $y_t \in O$, where $|O| = c$ and $O = \{1, \dots, c\}$.

Thus, an HMM is uniquely defined by a k -length initial probability vector π , $k \times k$ transition matrix \mathbf{P} , and $k \times c$ emission matrix Ψ . Entry i in the vector π is the probability of starting in state i , row i in the matrix \mathbf{P} is the state transition probability distribution from state i , and row i of the matrix Ψ is the emission distribution from state i .

HMMs are fit via the Baum-Welch algorithm, which identifies the parameters that (locally) maximize the likelihood of the observed data [1]. The likelihood of an observation sequence \mathbf{y} is a function of an HMM’s initial state distribution (π), transition probability matrix (\mathbf{P}), and emission matrix (Ψ) [20]. Let $\text{diag}(\Psi_i)$ be a $k \times k$ diagonal matrix with the i th column of Ψ as its entries - that is, the probabilities of observation i from each of the k states. Therefore, we have

$$\Pr(\mathbf{y} | \pi, \mathbf{P}, \Psi) = \pi^\top \cdot \text{diag}(\Psi_{y_0}) \cdot \left(\prod_{t=1}^T \mathbf{P} \cdot \text{diag}(\Psi_{y_t}) \right) \cdot \mathbf{1}_{k \times 1}. \quad (1)$$

3.2 Definition of hidden Markov recurrent neural networks (HMRNNs)

An HMRNN is a recurrent neural network whose parameters directly correspond to the initial state, transition, and emission probabilities of an HMM. As such, training an HMRNN optimizes the joint log-likelihood of the N T -length observation sequences given these parameters.

Definition 3.1. *An HMRNN is a recurrent neural network with trainable parameters π (a k -length stochastic vector), \mathbf{P} (a $k \times k$ stochastic matrix), and Ψ (a $k \times c$ stochastic matrix). It is trained on $T + 1$ input matrices of size $N \times c$, denoted by \mathbf{Y}_t for $t \in \{0, 1, \dots, T\}$, where the n -th row of matrix \mathbf{Y}_t is a one-hot encoded vector of observation $y_t^{(n)}$ for sequence $n \in \{1, \dots, N\}$. The HMRNN consists of an inner block of hidden layers that is looped $T + 1$ times (for $t \in \{0, 1, \dots, T\}$), with each loop containing hidden layers $\mathbf{h}_1^{(t)}$, $\mathbf{h}_2^{(t)}$, and $\mathbf{h}_3^{(t)}$, and a c -length input layer $\mathbf{h}_y^{(t)}$ through which the input matrix \mathbf{Y}_t enters the model. The HMRNN has a single output unit $o^{(T)}$ whose value is the joint negative log-likelihood of the N observation sequences under an HMM with parameters π , \mathbf{P} , and Ψ ; the summed value of $o^{(T)}$ across all N observation sequences is also the loss which is minimized through any neural network optimizer (e.g., gradient descent).*

Layers $\mathbf{h}_1^{(t)}$, $\mathbf{h}_2^{(t)}$, $\mathbf{h}_3^{(t)}$, and $o^{(T)}$ are defined in the following equations. Note that the block matrix in equation (3) is a $c \times (kc)$ block matrix of $c \mathbf{1}_{1 \times k}$ vectors, arranged diagonally, while the block

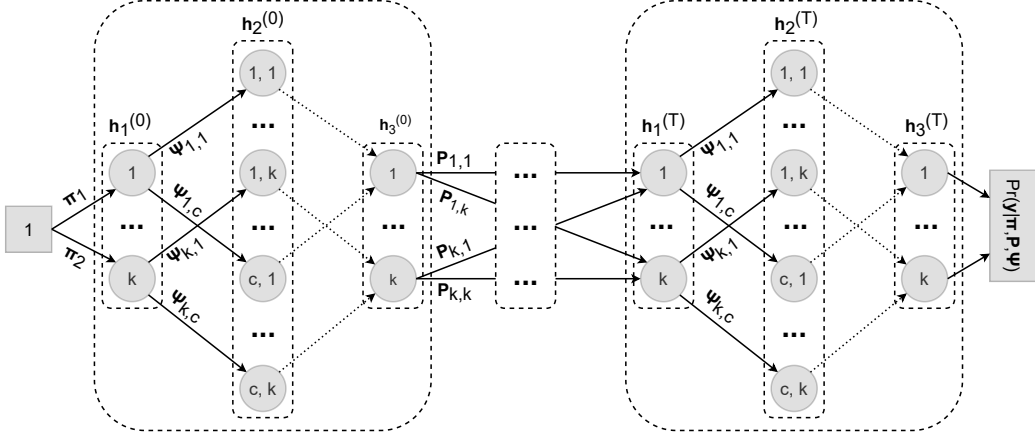


Figure 1: Structure of the hidden Markov recurrent neural network (HMRNN). Solid lines indicate learned weights that correspond to HMM parameters; dotted lines indicate weights fixed to 1. The inner block initializes with the initial state probabilities then mimics multiplication by Ψ ; connections between blocks mimic multiplication by P .

matrix in equation (4) is a $(kc) \times k$ row-wise concatenation of c $k \times k$ identity matrices.

$$\mathbf{h}_1^{(t)} = \begin{cases} \pi^\top, & t = 0, \\ \mathbf{h}_3^{(t-1)} \mathbf{P}, & t > 0. \end{cases} \quad (2)$$

$$\mathbf{h}_2^{(t)} = \text{ReLU} \left(\mathbf{h}_1^{(t)} [\text{diag}(\Psi_1) \dots \text{diag}(\Psi_c)] + \mathbf{Y}_t \begin{bmatrix} \mathbf{1}_{1 \times k} & \dots & \mathbf{0}_{1 \times k} \\ \dots & \dots & \dots \\ \mathbf{0}_{1 \times k} & \dots & \mathbf{1}_{1 \times k} \end{bmatrix} - \mathbf{1}_{n \times (kc)} \right) \quad (3)$$

$$\mathbf{h}_3^{(t)} = \mathbf{h}_2^{(t)} [\mathbf{I}_k \ \dots \ \mathbf{I}_k]^\top \quad (4)$$

$$o^{(T)} = -\log(\mathbf{h}_3^{(t)} \mathbf{1}_{k \times 1}). \quad (5)$$

Fig. 1 outlines the structure of the HMRNN. Intuitively, operations within each recurrent block mimic matrix multiplication by $\text{diag}(\Psi_{y_t})$ (i.e., $\mathbf{h}_3^{(t)} = \mathbf{h}_1^{(t)} \text{diag}(\Psi_{y_t})$), while connections between blocks mimic multiplication by P . In each block, layer $\mathbf{h}_1^{(t)}$ contains k units that represent the probability of being in each state $1-k$, given all past observations. Layer $\mathbf{h}_2^{(t)}$, expands each unit in $\mathbf{h}_1^{(t)}$ into c units via connections with weights $\Psi_{i,j}$ for $i \in \{1, \dots, k\}$ and $j \in \{1, \dots, c\}$, resulting in $k \cdot c$ units; this is equivalent to multiplying $\mathbf{h}_1^{(t)}$ (in row-vector form) by a column-wise concatenation of $\text{diag}(\Psi_j)$ for $j \in \{1, \dots, c\}$. The resulting units represent the probabilities of all possible state/outcome combinations at time t .

Layer $\mathbf{h}_2^{(t)}$ takes two more inputs: A bias unit (set to -1), and \mathbf{Y}_t , a one-hot encoded $n \times c$ matrix of data for time t , with each row a one-hot encoded vector of the observation for sequence n at time t . Each column in \mathbf{Y}_t is connected to all units in $\mathbf{h}_2^{(t)}$ that correspond to that column's observation, with connection weights set to 1. This is equivalent to multiplying \mathbf{Y}_t by a $k \times c$ block matrix of $c \mathbf{1}_{1 \times k}$ vectors, arranged diagonally. A ReLU activation is then applied to the layer; this leaves the units that correspond to \mathbf{Y}_t unchanged, while all other units (i.e., probabilities for non-occurring observations) are made negative by the -1 bias, then forced to zero through the ReLU activation. Thus, layer $\mathbf{h}_2^{(t)}$ identifies the joint probability of being in each state *and* observing \mathbf{Y}_t . Layer $\mathbf{h}_3^{(t)}$ then sums across all c units for each of the k states (all of which are zero except for those corresponding to \mathbf{Y}_t), yielding k units; this is equivalent to multiplying $\mathbf{h}_2^{(t)}$ by a row-wise concatenation of c $k \times k$ identity matrices. The k units in layer $\mathbf{h}_3^{(t)}$ now represent the probabilities of being in each state given all previous observations *and* the observation at time t , i.e., $\mathbf{h}_3^{(t)} = \mathbf{h}_1^{(t)} \text{diag}(\Psi_{y_t})$.

We then apply a fully-connected layer of weights to transform $\mathbf{h}_3^{(3)}$ to $\mathbf{h}_1^{(t+1)}$, equivalent to matrix multiplication by P , i.e., $\mathbf{h}_1^{(t+1)} = \mathbf{h}_3^{(t)} P$. Lastly, activations for $\mathbf{h}_3^{(T)}$ are summed into unit $o^{(T)}$

and subject to a negative logarithmic activation function, yielding the negative log-likelihood of the data given the model's parameters.

The HMRNN is a special case of an RNN, due to its time-dependent layers and shared weights between time points. Note that its use of recurrent blocks (each of which containing three layers) differs from many RNNs that use only a single layer at each time point; this distinction allows the HMRNN to mimic HMM computations of an HMM at each time point.

3.3 Proof of HMM/HMRNN Equivalence

We now formally establish that the HMRNN's output unit, $o^{(T)}$, is the negative log-likelihood of an observation sequence under an HMM with parameters π , P , and Ψ . We prove this for the case of $N = 1$ and drop notational dependence on n (i.e., we write $y_t^{(1)}$ as y_t), though extension to $N > 1$ is trivial since the log-likelihood of multiple independence sequences is simply the sum of their individual log-likelihoods. We first rely on the following lemmas, which together prove that each recurrent block of the HMRNN mimics matrix multiplication by $\text{diag}(\Psi_{y_t})$, given some observation y_t at time t .

Lemma 3.1. *Let unit $\mathbf{h}_1^{(t)}(j)$ represent the j th unit of $\mathbf{h}_1^{(t)}(j)$. If $\mathbf{h}_1^{(t)}(j) \in [0, 1]$ for $j \in \{1, \dots, k\}$, then $\mathbf{h}_3^{(t)} = \mathbf{h}_1^{(t)} \text{diag}(\Psi_{y_t})$.*

Proof. Let $\mathbf{h}_1^{(t)}(j)$ and $\mathbf{h}_3^{(t)}(j)$ represent the j th units of layer $\mathbf{h}_1^{(t)}$ and $\mathbf{h}_3^{(t)}$, respectively. Showing $\mathbf{h}_3^{(t)} = \mathbf{h}_1^{(t)} \text{diag}(\Psi_{y_t})$ is equivalent to showing that $\mathbf{h}_3^{(t)}(j) = \Psi_{j, y_t} \mathbf{h}_1^{(t)}(j)$ for $j \in \{1, \dots, k\}$.

To show this, recall that $\mathbf{h}_2^{(t)}$ contains $k \times c$ units, which we index with a tuple (l, m) for $l \in \{1, \dots, c\}$ and $m \in \{1, \dots, k\}$. The connection matrix between $\mathbf{h}_1^{(t)}$ and $\mathbf{h}_2^{(t)}$ is $[\text{diag}(\Psi_1) \dots \text{diag}(\Psi_c)]$. Thus, the connection between units $\mathbf{h}_1^{(t)}(j)$ and $\mathbf{h}_2^{(t)}(l, m)$ is $\Psi_{j, l}$ when $j = m$, and equals 0 otherwise. Also recall that matrix \mathbf{Y}_t enters the model through a c -length input layer $\mathbf{h}_y^{(t)}$, where the j th unit is 1 when $y_t = j$, and equals 0 otherwise. This layer is connected to $\mathbf{h}_2^{(t)}$ by a $c \times (kc)$ diagonal block matrix of c ($1 \times k$) row vectors of ones. Thus, the connection between the j th unit of this input layer and unit (l, m) of $\mathbf{h}_2^{(t)}$ is 1 when $j = l$, and equals 0 otherwise. Lastly, a bias of -1 is added to all units in $\mathbf{h}_2^{(t)}$, which is then subject to a ReLu activation, resulting in the following expression for each unit in $\mathbf{h}_2^{(t)}$:

$$\mathbf{h}_2^{(t)}(l, m) = \text{ReLU}(\Psi_{m, l} \cdot \mathbf{h}_1^{(t)}(m) + \mathbf{h}_y^{(t)}(l) - 1) \quad (6)$$

Because $\mathbf{h}_y^{(t)}(l)$ is 1 when $y_t = l$, and equals 0 otherwise, then if all units in $\mathbf{h}_1^{(t)}$ are between 0 and 1, we have

$$\mathbf{h}_2^{(t)}(l, m) = \begin{cases} \text{ReLU}(\Psi_{m, l} \cdot \mathbf{h}_1^{(t)}(m)) = \Psi_{m, l} \cdot \mathbf{h}_1^{(t)}(m), & j = y_t, \\ \text{ReLU}(\Psi_{m, l} \cdot \mathbf{h}_1^{(t)}(m) - 1) = 0, & \text{otherwise.} \end{cases} \quad (7)$$

The connection matrix between $\mathbf{h}_2^{(t)}$ and $\mathbf{h}_3^{(t)}$ is a $(kc) \times k$ row-wise concatenation of $k \times k$ identity matrices; thus, the connection between $\mathbf{h}_2^{(t)}(l, m)$ and $\mathbf{h}_3^{(t)}(j)$ is 1 if $j = m$, and 0 otherwise. Hence,

$$\mathbf{h}_3^{(t)}(j) = \sum_{l=0}^c \mathbf{h}_2^{(t)}(l, j) = \Psi_{j, y_t} \cdot \mathbf{h}_1^{(t)}(j). \quad (8)$$

□

Thus, $\mathbf{h}_3^{(t)} = \mathbf{h}_1^{(t)} \text{diag}(\Psi_{y_t})$.

Lemma 3.2. *For all $j \in \{1, \dots, k\}$ and $t \in \{0, \dots, T\}$, $\mathbf{h}_1^{(t)}(j) \in [0, 1]$.*

Proof. We show this by induction. We first assume that for some time t , $0 \leq \mathbf{h}_1^{(t)}(j) \leq 1$ for all j and $\sum_{j=1}^k \mathbf{h}_1^{(t)}(j) \leq 1$. Given that $\mathbf{h}_3^{(t)}(j) = \Psi_{j, y_t} \cdot \mathbf{h}_1^{(t)}(j)$ and $0 \leq \Psi_{i, j} \leq 1$ for all i and j ,

then $0 \leq \mathbf{h}_3^{(t)}(j) \leq 1$ for all j and $\sum_{j=1}^k \mathbf{h}_3^{(t)}(j) \leq 1$. Since $\mathbf{h}_1^{(t+1)} = \mathbf{h}_3^{(t)} \mathbf{P}$ and $0 \leq \mathbf{P}_{i,j} \leq 1$ for all i and j , then $0 \leq \mathbf{h}_1^{(t+1)}(j) \leq 1$ for all j and $\sum_{j=1}^k \mathbf{h}_1^{(t+1)}(j) \leq 1$. Since $\mathbf{h}_1^{(0)} = \boldsymbol{\pi}^\top$, then $0 \leq \mathbf{h}_1^{(t)}(j) \leq 1$ and $\sum_{j=1}^k \mathbf{h}_1^{(t)}(j) \leq 1$ for $t = 0$, implying $0 \leq \mathbf{h}_1^{(t)}(j) \leq 1$ for all j and t . \square

Theorem 3.1. *An HMRNN with parameters $\boldsymbol{\pi}$ ($1 \times k$ stochastic vector), \mathbf{P} ($k \times k$ stochastic matrix), and $\boldsymbol{\Psi}$ ($k \times c$ stochastic matrix), and with layers defined as in equations (2-5), produces output neuron $o^{(T)}$ for sequence $n \in \{1, \dots, N\}$ whose value is the negative log-likelihood of a corresponding HMM as defined in equation (1).*

Proof. Taken together, Lemmas 3.1 and 3.2 imply that $\mathbf{h}_3^{(t)} = \mathbf{h}_1^{(t)} \text{diag}(\boldsymbol{\Psi}_{y_t})$ for all t , while $\mathbf{h}_1^{(t+1)} = \mathbf{h}_3^{(t)} \mathbf{P}$. Thus, $\mathbf{h}_3^{(t)} = \mathbf{h}_3^{(t-1)}(\mathbf{P} \cdot \text{diag}(\boldsymbol{\Psi}_{y_t}))$ for $t \in \{1, \dots, T\}$. Thus, we can express output neuron $o^{(T)}$ recursively as $o^{(T)} = -\log(\mathbf{h}_3^{(t)} \mathbf{1}_{k \times 1}) = -\log(\mathbf{h}_3^{(0)}(\prod_{t=1}^T \mathbf{P} \cdot \text{diag}(\boldsymbol{\Psi}_{y_t})) \mathbf{1}_{k \times 1})$. Lastly, for $t = 0$, $\mathbf{h}_1^{(0)} = \boldsymbol{\pi}^\top$; thus, $\mathbf{h}_3^{(0)} = \boldsymbol{\pi}^\top \cdot \text{diag}(\boldsymbol{\Psi}_{y_0})$, and $o^{(T)} = -\log(\boldsymbol{\pi}^\top \cdot \text{diag}(\boldsymbol{\Psi}_{y_0}) \cdot (\prod_{t=1}^T \mathbf{P} \cdot \text{diag}(\boldsymbol{\Psi}_{y_t})) \mathbf{1}_{k \times 1})$, which is identical to the HMM likelihood from equation (1). \square

4 Experiments and Results

In this section, we compare HMRNNs to HMMs through computational experiments with synthetic data and a case study of real-world clinical data from Alzheimer’s disease patients.

4.1 Empirical Validation of HMRNN

We confirm numerically that an HMRNN trained via gradient descent yields statistically similar solutions to the Baum-Welch algorithm. We show this with synthetically-generated observation sequences for which the true HMM parameters are known, allowing us to assess each algorithm’s ability to recover the true model parameters.

We simulate two-state systems where each row of the transition and emission matrices is set to either $[0.05, 0.95]$ or $[0.33, 0.67]$, for a total of $2^4 = 16$ HMM’s. This allows us to test a “strong” and “weak” case, respectively, for each probability/emission distribution (i.e., where the most likely outcome is either near-certain, or only occurs with 2/3 probability). For each of the 16 HMMs, we generate two 200-length synthetic observation sequences on which the Baum-Welch and HMRNN are trained; one sequence for each HMM starts in state $x_0 = 0$, while the other starts in state $x_0 = 1$ (32 sequences in total). We train the HMM and HMRNN on 10 random initializations for each synthetic sequence and select the best-performing (i.e., highest log-likelihood) parameter solution, yielding 32 finalized parameter solutions for comparison. Convergence is defined as all parameter estimates ceasing to change by more than 0.0001. For analysis purposes, we define transition parameter solutions as $[\min(\mathbf{P}_{11}, \mathbf{P}_{22}), \max(\mathbf{P}_{11}, \mathbf{P}_{22})]^\top$, i.e., an ordered pair of the same-state transition probabilities, which fully characterizes the 2×2 transition probability matrix. We define emission parameter solutions as $[\min(\boldsymbol{\Psi}_{11}, \boldsymbol{\Psi}_{12}), \max(\boldsymbol{\Psi}_{11}, \boldsymbol{\Psi}_{12})]^\top$, i.e., an ordered pair of the probabilities of observing $y_{t(n)} = 0$, which fully characterizes the 2×2 emission matrix.

Fig. 2 shows the log-likelihoods and parameter estimates for Baum-Welch and HMRNN parameter solutions. Solutions across both models yield similar log-likelihoods (correlation $r = 0.997$), and for 21 of the 32 model runs, transition and emission solutions differ by no more than 0.05 on any parameter. A nonparametric multivariate test based on the energy distance ([21, 22]) finds no significant differences between the Baum-Welch and HMRNN distributions of transition (p -value = 0.40) or emission (p -value = 0.90) parameter solutions. The Baum-Welch and HMRNN solutions also do not significantly differ in the Kullback-Leibler divergence between estimated and ground truth transition distributions (Mann-Whitney U test, p -value = 0.29) or emission distributions (Mann-Whitney U test, p -value = 0.27).

Moreover, Fig. 2(b) and Fig. 2(c) show that the medians of Baum-Welch and HMRNN parameter solutions are close to the ground truth parameters, thus conforming empirically that the HMRNN recovers the true parameters used to generate each observation sequence.

The median runtime for Baum-Welch across all model runs is 1.93 seconds, versus 64.28 seconds for gradient descent with the HMRNN. This runtime difference reflects the fact that the HMRNN is

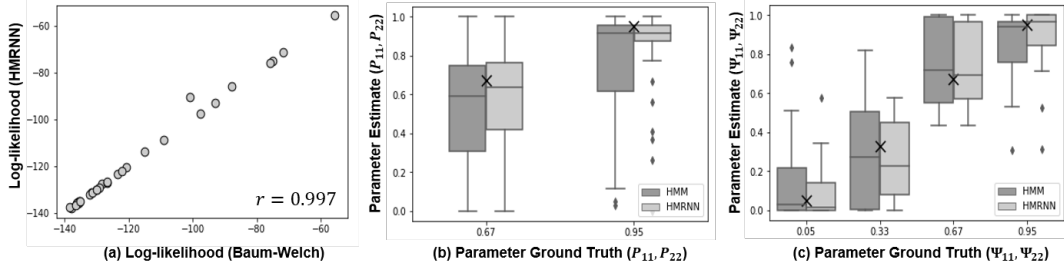


Figure 2: Comparison of HMM Baum-Welch and HMRNN gradient descent solutions for synthetic data experiments. (a) Agreement of log-likelihoods between HMM/Baum-Welch and HMRNN/gradient descent. (b) Box plots of same-state transition parameters. Ground truth parameters marked by crosses. (c) Box plots of emission parameters for $\Pr(y_t^{(n)} = 0)$. Ground truth parameters marked by crosses.

fitting a very deep (600–layer) neural network, while the Baum-Welch algorithm is tailor-made for the HMM data structure. Still, this emphasizes that any benefit of the HMRNN model should lie in its ability to handle data structures inaccessible to the Baum-Welch algorithm, rather than its speed.

4.2 Alzheimer’s disease symptom progression data

We apply an HMRNN and augment it with other neural networks in a case study of Alzheimer’s disease symptom progression. In doing so, we demonstrate how combining an HMRNN with other neural networks can improve parameter fit and offer novel clinical interpretations.

We test our HMRNN on clinical data from $n = 426$ patients with mild cognitive impairment (MCI), collected over the course of three ($n = 91$), four ($n = 106$), or five ($n = 229$) consecutive annual clinical visits. Data was taken from the Alzheimer’s Disease Neuroimaging Initiative [23]. Given MCI patients’ heightened risk of Alzheimer’s, modeling their symptom progression is of considerable clinical interest [24, 25, 26]. We analyze patients’ level of functional independence based on the Functional Activities Questionnaire (FAQ; [27]) and overall cognitive functioning based on the Mini Mental Status Exam (MMSE; [28]). FAQ scores range from 0 to 30, with scores of 9 – 30 indicating impaired functioning and 0 – 8 indicating normal functioning. MMSE scores range from 0 to 30, with scores of 27 – 30 indicating no cognitive impairment, 24 – 26 indicating borderline cognitive impairment, and 17 – 23 indicating mild cognitive impairment [29, 30]. The proportion of scores below 17 (1.2%) were insufficient for analysis of a separate diagnostic category, and these scores were treated as scores of 17 (‘mild cognitive impairment’) for analysis purposes.

For FAQ analysis, we define the latent space as $S = \{0, 1\}$, with $x_t = 0$ representing ‘normal functioning’ and $x_t = 1$ representing ‘impaired functioning.’ We define the observation space as $O = \{0, 1\}$, with $y_t = 0$ representing an FAQ score below 9 and $y_t = 1$ representing an FAQ score of 9 or higher. For MMSE analysis, we define the latent space as $S = \{0, 1, 2\}$, with $x_t = 0$ representing ‘no cognitive impairment,’ $x_t = 1$ representing ‘borderline cognitive impairment,’ and $x_t = 2$ representing ‘mild cognitive impairment.’ The observation space is $O = \{0, 1, 2\}$, with $y_t = 0$ representing an MMSE score of 27 – 30, $y_t = 1$ representing an MMSE score of 24 – 26, and $y_t = 2$ representing an MMSE score of 17 – 23.

To showcase the benefits of the HMRNN’s flexibility, we train three models each for the FAQ and MMSE: a baseline HMM (using Baum-Welch), a baseline HMRNN, and an augmented HMRNN. The baseline HMM and HMRNN simply learn the initial state probabilities, and the transition and emission matrices from the $n = 426$ patient sequences. The augmented HMRNN showcases the HMRNN’s flexibility through two substantive modifications. First, the initial state probabilities in the augmented HMRNN are predicted from patients’ gender, age, degree of temporal lobe atrophy [31], and amyloid-beta 42 levels ($A\beta42$, a relevant Alzheimer’s biomarker [32, 33]), using a single-layer neural network. Second, at each time point, the probability of being in the most impaired state ($h_t^{(1)}$ for FAQ, $h_t^{(1)}$ for MMSE) is used to predict concurrent scores on the Clinical Dementia Rating (CDR, [34]), a global assessment of dementia severity, allowing another clinical metric to inform estimation. We use a single connection and sigmoid activation to predict patients’ probability

	HMM		HMRNN (baseline)		HMRNN (augmented)	
π	0.909	0.091	0.912	0.088	0.946	0.054
P	0.918	0.082	0.923	0.076	0.918	0.082
	0.030	0.970	0.014	0.986	0.007	0.993
Ψ	0.981	0.019	0.969	0.031	0.982	0.018
	0.037	0.963	0.037	0.963	0.056	0.944
LL	-905.32		-899.84		-861.71	
Runtime	2.16 sec		2.73 sec		13.54 sec	

Table 1: Results from Alzheimer’s disease case study (Functional Activities Questionnaire). Note that π indicates initial state probabilities, P indicates transition probability matrix, Ψ indicates emission matrix, and LL indicates model log-likelihood. For transition probability matrices, element (i, j) is the probability of transitioning from state i to state j . For emission matrices, element (i, j) is the probability of making observation j from latent state i .

	HMM			HMRNN (baseline)			HMRNN (augmented)		
π	0.727	0.271	0.002	0.730	0.269	0.001	0.667	0.333	0.000
P	0.898	0.080	0.022	0.900	0.085	0.015	0.970	0.028	0.002
	0.059	0.630	0.311	0.077	0.617	0.305	0.006	0.667	0.327
	0.000	0.016	0.984	0.002	0.027	0.971	0.000	0.003	0.997
Ψ	0.939	0.060	0.001	0.927	0.057	0.016	0.930	0.067	0.003
	0.175	0.819	0.006	0.144	0.835	0.021	0.449	0.548	0.003
	0.004	0.160	0.836	0.014	0.142	0.844	0.005	0.308	0.687
LL	-1545.52			-1549.51			-1353.16		
Runtime	2.89 sec			5.18 sec			15.24 sec		

Table 2: Results from Alzheimer’s disease case study (Mini Mental Status Exam). Note that π indicates initial state probabilities, P indicates transition probability matrix, Ψ indicates emission matrix, and LL indicates model log-likelihood. For transition probability matrices, element (i, j) is the probability of transitioning from state i to state j . For emission matrices, element (i, j) is the probability of making observation j from latent state i .

of receiving a CDR score above 0.5 (corresponding to ‘mild dementia’). We train all models using a log-likelihood tolerance of 0.001% (we do not use parameter convergence since the number of parameters differs across models).

FAQ model results appear in Table 1, and MMSE model results appear in Table 2. For both assessments, augmenting the HMRNN with other neural networks improves fit and produces different parameter interpretations. For FAQ data, the augmented HMRNN yields the highest starting probability for functional impairment and the lowest probability of recovery this state. It also infers the highest FAQ false negative rate – a 5.6% chance of impaired patients scoring as ‘normal’ ($\Psi_{21} = 0.056$, Table 1). Thus, under the augmented HMRNN, patients are more likely to occupy the ‘functional impairment’ state, and FAQ scores of 0 – 8 are more likely to be attributed to false negatives (rather than a ‘normal’ level of functioning). For MMSE data, the augmented HMRNN yields the lowest transition probabilities between states and the lowest MMSE diagnostic accuracy. For instance, the baseline HMM and HMRNN estimate at least an 80% chance of correctly identifying borderline and mild cognitive impairment; that is, $\Psi_{22} = 0.819$ and $\Psi_{33} = 0.836$ for FAQ, and $\Psi_{22} = 0.835$ and $\Psi_{33} = 0.844$ for MMSE (Table 2). These probabilities are (respectively) only 54.8% and 68.7% under the HMRNN, suggesting that changes in scores are more likely attributable to testing error (as opposed to true state changes) under the augmented HMRNN.

5 Discussion

We outline a flexible approach for HMM parameter estimation using neural networks. The HMRNN produces statistically similar solutions to the Baum-Welch algorithm, yet can be combined with other neural networks to improve parameter estimates. In our case study, the augmented HMRNN yields higher log-likelihoods and different clinical interpretations than the baseline HMMs. For the FAQ, it suggests a higher initial probability for ‘impaired’ functioning and a higher assessment false negative

rate (5.6%), which, interestingly, is closer to other false negative rates for MCI screenings that rely on the FAQ (7.1%, [35]), compared with the baseline HMMs. For the MMSE, the augmented HMRNN estimates relatively poor diagnostic accuracy for the ‘borderline’ and ‘mild’ cognitive impairment states, suggesting that fewer diagnostic categories might improve the MMSE’s utility (as supported by existing MMSE research, e.g., [30]).

In addition to demonstrating the HMRNN’s utility in a practical setting, we also make a theoretical contribution by formulating discrete-observation HMMs as a special case of RNNs and by proving coincidence of likelihood functions between the two formulations. Unlike past approaches, our formulation relies only on matrix multiplication and ReLu activations, and is designed to for generalized use by optimizing for maximum likelihood, which is widely used for HMM training.

Future work may attempt to speed up the HMRNN approach to reach runtime parity with Baum-Welch. It is worth noting that sequence lengths in healthcare are often considerably shorter than in other domains that employ HMMs (e.g., speech analysis), and runtimes will likely remain reasonable for many healthcare datasets. We also limited our practical case study to disease progression modeling, while future work might explore HMRNN variants in other healthcare domains.

Acknowledgments and Disclosure of Funding

This research is partially supported by the Joint Directed Research and Development program at Science Alliance, University of Tennessee.

Data collection and sharing for this project was funded by the Alzheimer’s Disease Neuroimaging Initiative (ADNI) (National Institutes of Health Grant U01 AG024904) and DOD ADNI (Department of Defense award number W81XWH-12-2-0012). ADNI is funded by the National Institute on Aging, the National Institute of Biomedical Imaging and Bioengineering, and through generous contributions from the following: AbbVie, Alzheimer’s Association; Alzheimer’s Drug Discovery Foundation; Araclon Biotech; BioClinica, Inc.; Biogen; Bristol-Myers Squibb Company; CereSpir, Inc.; Cogstate; Eisai Inc.; Elan Pharmaceuticals, Inc.; Eli Lilly and Company; EuroImmun; F. Hoffmann-La Roche Ltd and its affiliated company Genentech, Inc.; Fujirebio; GE Healthcare; IXICO Ltd.; Janssen Alzheimer Immunotherapy Research & Development, LLC.; Johnson & Johnson Pharmaceutical Research & Development LLC.; Lumosity; Lundbeck; Merck & Co., Inc.; Meso Scale Diagnostics, LLC.; NeuroRx Research; Neurotrack Technologies; Novartis Pharmaceuticals Corporation; Pfizer Inc.; Piramal Imaging; Servier; Takeda Pharmaceutical Company; and Transition Therapeutics. The Canadian Institutes of Health Research is providing funds to support ADNI clinical sites in Canada. Private sector contributions are facilitated by the Foundation for the National Institutes of Health (www.fnih.org). The grantee organization is the Northern California Institute for Research and Education, and the study is coordinated by the Alzheimer’s Therapeutic Research Institute at the University of Southern California. ADNI data are disseminated by the Laboratory for Neuro Imaging at the University of Southern California.

This manuscript has been authored by UT-Battelle, LLC, under contract DE-AC05-00OR22725 with the US Department of Energy (DOE). The US government retains and the publisher, by accepting the article for publication, acknowledges that the US government retains a nonexclusive, paid-up, irrevocable, worldwide license to publish or reproduce the published form of this manuscript, or allow others to do so, for US government purposes. DOE will provide public access to these results of federally sponsored research in accordance with the DOE Public Access Plan (<http://energy.gov/downloads/doe-public-access-plan>). This research was sponsored by the Laboratory Directed Research and Development Program of Oak Ridge National Laboratory, managed by UT-Battelle, LLC, for the US Department of Energy under contract DE-AC05-00OR22725.

References

- [1] L.E. Baum and T. Petrie. Statistical inference for probabilistic functions of finite state Markov chains. *The Annals of Mathematical Statistics*, 37(6):1554–1563, 1966.
- [2] C. Guiheneuc-Jouyaux, S. Richardson, and I.M. Longini Jr. Modeling markers of disease progression by a hidden Markov process: Application to characterizing CD4 cell decline. *Biometrics*, 56(3):733–741, 2000.

- [3] Y.Y. Liu, S. Li, F. Li, L. Song, and J.M. Rehg. Efficient learning of continuous-time hidden Markov models for disease progression. *Advances in Neural Information Processing Systems*, pages 3600–3608, 2015.
- [4] T. Ayer, O. Alagoz, and N.K. Stout. A POMDP approach to personalize mammography screening decisions. *Operations Research*, 60(5):1019–1034, 2012.
- [5] S. Nemati, M.M. Ghassemi, and G.D. Clifford. Optimal medication dosing from suboptimal clinical examples: A deep reinforcement learning approach. *38th Annual International Conference of IEEE Engineering in Medicine and Biology Society*, pages 2978–2981, 2016.
- [6] M. Igl, L. Zintgraf, T.A. Le, F. Wood, and S. Whiteson. Deep variational reinforcement learning for POMDPs. *arXiv preprint*, 2018.
- [7] A. Gupta. Developing clinical decision support systems for sepsis prediction using temporal and non-temporal machine learning method. *Unpublished doctoral dissertation*, 2019.
- [8] Z. Zhou, Y. Wang, H. Mamani, and D.G. Coffey. How do tumor cytogenetics inform cancer treatments? dynamic risk stratification and precision medicine using multi-armed bandits. *Preprint*, 2019.
- [9] J.S. Bridle. Alpha-nets: A recurrent ‘neural’ network architecture with a hidden Markov model interpretation. *Speech Communication*, 9(1):83–92, 1990.
- [10] M. Fuentes, S. Garcia-Salicetti, and B. Dorizzi. *Online signature verification: Fusion of a hidden Markov model and a neural network via a support vector machine*, pages 253–258. IEEE, 2002.
- [11] V. Krakovna and F. Doshi-Velez. Increasing the interpretability of recurrent neural networks using hidden Markov models. *arXiv preprint*, 2016.
- [12] S. Knerr and E. Augustin. *A neural network-hidden Markov model hybrid for cursive word recognition*, volume 2, pages 1518–1520. IEEE, 1998.
- [13] Y. Bengio, R. De Mori, G. Flammia, and R. Kompe. Global optimization of a neural network-hidden Markov model hybrid. *IEEE Transactions on Neural Networks*, 3(27):252–259, 1992.
- [14] Ingmar Visser, Maartje EJ Raijmakers, and Peter CM Molenaar. *Hidden Markov model interpretations of neural networks*, pages 197–206. Springer, 2001.
- [15] T. Wessels and C.W. Omlin. Refining hidden Markov models with recurrent neural networks. In *Proceedings of the IEEE-INNS-ENNS International Joint Conference on Neural Networks*, volume 2, pages 271–276, 2000.
- [16] B. Estebanez, P. del Saz-Orozco, I. Rivas, E. Bauzano, V.F. Muñoz, and I. Garcia-Morales. *Maneuvers recognition in laparoscopic surgery: Artificial Neural Network and hidden Markov model approaches*, pages 1164–1169. IEEE, 2012.
- [17] M. Baucum, A. Khojandi, and R. Vasudevan. Improving deep reinforcement learning with transitional variational autoencoders: A health care application, 2020. Preprint.
- [18] M.I. Námen Leon. A POMDP approach to age-dependent primary screening policies for cervical cancer in colombia. *Unpublished Master’s thesis*, 2015.
- [19] I. Stanculescu, C.K. Williams, and Y. Freer. Autoregressive hidden Markov models for the early detection of neonatal sepsis. *IEEE Journal of Biomedical and Health Informatics*, 18(5):1560–1570, 2013.
- [20] D. Jurafsky and J. Martin. *Speech and language processing*. Pearson, 2009.
- [21] G.J. Szekely and M.L. Rizzo. The energy of data. *Annual Review of Statistics and its Application*, 4:447–479, 2017.
- [22] M.L. Rizzo and G.J. Szekely. Energy distance. *Wiley Interdisciplinary Reviews: Computational Statistics*, 8(1):27–38, 2016.

- [23] Alzheimer's disease neuroimaging initiative. adni.loni.usc.edu.
- [24] K. Hirao, T. Ohnishi, Y. Hirata, F. Yamashita, T. Mori, Y. Moriguchi, and T. Iwamoto. The prediction of rapid conversion to Alzheimer's disease in mild cognitive impairment using regional cerebral blood flow spect. *Neuroimage*, 28(4):1014–1021, 2005.
- [25] Oskar Hansson, Henrik Zetterberg, Eugeen Vanmechelen, Hugo Vanderstichele, Ulf Andreasson, Elisabet Londos, Anders Wallin, Lennart Minthon, and Kaj Blennow. Evaluation of plasma $\alpha\beta40$ and $\alpha\beta42$ as predictors of conversion to alzheimer's disease in patients with mild cognitive impairment. *Neurobiology of aging*, 31(3):357–367, 2010.
- [26] L.A. Rabin, N. Pare, A.J. Saykin, M.J. Brown, H.A. Wishart, L.A. Flashman, and R.B. Santulli. Differential memory test sensitivity for diagnosing amnestic mild cognitive impairment and predicting conversion to alzheimer's disease. *Aging, Neuropsychology, and Cognition*, 16(3):357–376, 2009.
- [27] R.I. Pfeffer, T.T. Kurosaki, Jr. C.H. Harrah, J.M. Chance, and S. Filos. Measurement of functional activities in older adults in the community. *Journal of Gerontology*, 37(3):323–329, 1982.
- [28] M.F. Folstein, S.E. Folstein, and P.R. McHugh. Mini-mental state: A practical method for grading the cognitive state of patients for the clinician. *Journal of Psychiatric Research*, 12(3):189–198, 1975.
- [29] A. Chopra, T.A. Cavalieri, and D.J. Libon. Dementia screening tools for the primary care physician. *Clinical Geriatrics*, 15(1):38–45, 2007.
- [30] T. Monroe and M. Carter. Using the Folstein mini mental state exam (MMSE) to explore methodological issues in cognitive aging research. *European Journal of Ageing*, 9(3):265–274, 2012.
- [31] X. Hua, A.D. Leow, S. Lee, A.D. Klunder, A.W. Toga, N. Lepore, Y. Chou, C. Brun, M. Chiang, M. Barysheva, Jr. C.R. Jack, M.A. Bernstein, P.J. Britson, C.P. Ward, J.L. Whitwell, B. Borowski, A. Fleisher, N.C. Fox, R.G. Boyes, J. Barnes, D. Harvey, J. Kornak, N. Schuff, L. Boreta, G.E. Alexander, M.W. Weiner, and P.M. Thompson. 3d characterization of brain atrophy in Alzheimer's disease and mild cognitive impairment using tensor-based morphometry. *Neuroimage*, 41(1):19–34, 2008.
- [32] L. Canuet, S. Pusil, M.E. Lopez, R. Bajo, J.A. Pineda-Pardo, P. Cuesta, G. Galvez, J.M. Gatzelu, D. Lourido, G. Garcia-Ribas, and F. Maestu. Network disruption and cerebrospinal fluid amyloid-beta and phospho-tau levels in mild cognitive impairment. *Journal of Neuroscience*, 35(28):10325–10330, 2015.
- [33] K. Blennow. Cerebrospinal fluid protein biomarkers for Alzheimer's disease. *NeuroRx*, 1(2):213–225], 2004.
- [34] J.C. Morris. Clinical dementia rating: Current version and scoring rules. *Neurology*, 43:2412–2414, 1993.
- [35] E.C. Edmonds, L. Delano-Wood, A.J. Jak, D.R. Galasko, D.P. Salmon, and M.W. Bondi. 'missed' mild cognitive impairment: High false-negative error rate based on conventional diagnostic criteria. *Journal of Alzheimer's Disease*, 52(2):685–691, 2016.